

Accepted Manuscript

Detection of neural connections with *ex vivo* MRI using a ferritin-encoding trans-synaptic virus

Ning Zheng, Peng Su, Yue Liu, Huadong Wang, Binbin Nie, Xiaohui Fang, Yue Xu, Kunzhang Lin, Pei Lv, Xiaobin He, Yi Guo, Baoci Shan, Anne Manyande, Jie Wang, Fuqiang Xu

PII: S1053-8119(19)30325-8

DOI: <https://doi.org/10.1016/j.neuroimage.2019.04.039>

Reference: YNIMG 15795

To appear in: *NeuroImage*

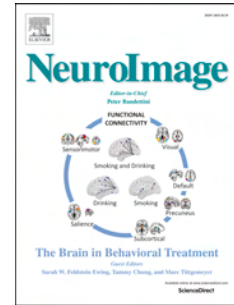
Received Date: 4 September 2018

Revised Date: 6 March 2019

Accepted Date: 11 April 2019

Please cite this article as: Zheng, N., Su, P., Liu, Y., Wang, H., Nie, B., Fang, X., Xu, Y., Lin, K., Lv, P., He, X., Guo, Y., Shan, B., Manyande, A., Wang, J., Xu, F., Detection of neural connections with *ex vivo* MRI using a ferritin-encoding trans-synaptic virus, *NeuroImage* (2019), doi: <https://doi.org/10.1016/j.neuroimage.2019.04.039>.

This is a PDF file of an unedited manuscript that has been accepted for publication. As a service to our customers we are providing this early version of the manuscript. The manuscript will undergo copyediting, typesetting, and review of the resulting proof before it is published in its final form. Please note that during the production process errors may be discovered which could affect the content, and all legal disclaimers that apply to the journal pertain.



Detection of neural connections with *ex vivo* MRI using a ferritin-encoding trans-synaptic virus

Ning Zheng^{a,b,1}, Peng Su^{c,1}, Yue Liu^a, Huadong Wang^a, Binbin Nie^{b,d}, Xiaohui Fang^a, Yue Xu^a, Kunzhang Lin^a, Pei Lv^a, Xiaobin He^a, Yi Guo^a, Baoci Shan^{b,d,e}, Anne Manyande^f, Jie Wang^{a,b,*}, Fuqiang Xu^{a,b,c,e,*}

^a State Key Laboratory of Magnetic Resonance and Atomic and Molecular Physics, Key Laboratory of Magnetic Resonance in Biological Systems, Wuhan Center for Magnetic Resonance, Wuhan Institute of Physics and Mathematics, Chinese Academy of Sciences, Wuhan 430071, P.R. China;

^b University of Chinese Academy of Sciences, Beijing, 100049, P.R. China;

^c Wuhan National Laboratory for Optoelectronics, Huazhong University of Science and Technology, Wuhan, 430074, China.

^d Key Laboratory of Nuclear Radiation and Nuclear Energy Technology, Institute of High Energy Physics, Chinese Academy of Sciences, Beijing 100049, P.R. China

^e Center for Excellence in Brain Science and Intelligent Technology, Chinese Academy of Sciences, Shanghai 200031, P.R. China;

^f School of Human and Social Sciences, University of West London, London, UK

Short title: Detection of neuronal connections with *ex vivo* MRI

¹: These authors contributed equally to this work

*: Corresponding author

Jie Wang, E-mail: jie.wang@wipm.ac.cn; Tel: +86-27-87187359; Fax: +86-27-87199543.

Fuqiang Xu, Email: fuqiang.xu@wipm.ac.cn; Tel: +86-27-87197091; Fax: +86-27-87199543

25 **Abstract:** The elucidation of neural networks is essential to understanding the mechanisms of brain
26 functions and brain disorders. Neurotropic virus-based trans-synaptic tracing tools have become an
27 effective method for dissecting the structure and analyzing the function of neural-circuitry. However, these
28 tracing systems rely on fluorescent signals, making it hard to visualize the panorama of the labeled
29 networks in mammalian brain *in vivo*. One MRI method, Diffusion Tensor Imaging (DTI), is capable of
30 imaging the networks of the whole brain in live animals but without information of anatomical connections
31 through synapses. In this report, a chimeric gene coding for ferritin and enhanced green fluorescent protein
32 (EGFP) was integrated into Vesicular stomatitis virus (VSV), a neurotropic virus that is able to spread
33 anterogradely in synaptically connected networks. After the animal was injected with the recombinant
34 VSV (rVSV), rVSV-Ferritin-EGFP, into the somatosensory cortex (SC) for four days, the labeled
35 neural-network was visualized in the postmortem whole brain with a T2-weighted MRI sequence. The
36 modified virus transmitted from SC to synaptically connected downstream regions. The results
37 demonstrate that rVSV-Ferritin-EGFP could be used as a bimodal imaging vector for detecting synaptically
38 connected neural-network with both *ex vivo* MRI and fluorescent imaging. The strategy in the current
39 study has the potential to longitudinally monitor the global structure of a given neural-network in living
40 animals.

41

42 **Keywords:** Ferritin; synaptically connected neural networks; MRI; fluorescent imaging; VSV

43 1. Introduction

44 The extremely complex neural circuit is the structural basis for all brain functions, such as
45 consciousness, cognition, emotion, learning and memory. Therefore, identifying and dissecting the
46 corresponding neural-circuit for a given function is a prerequisite for understanding the basic function of
47 the brain and the cause of neurological disorders (Tye and Deisseroth, 2012).

48 Currently, there are a few approaches that can be used to investigate the structure of neural circuits
49 (Lerner et al., 2016). Firstly, neural-circuit tracers, which can be efficiently taken up and actively
50 transported by neurons, have long been utilized to dissect the neural network. These tracers include
51 horseradish peroxidase (Paton and Nottebohm, 1984), fluoro-gold (Brog et al., 1993), wheat germ
52 agglutinin (Numan and Numan, 1997), tetanus cholera B fragment (Lai et al., 2015), barley lectin
53 (Horowitz et al., 1999) and neurotropic viruses (Callaway, 2008; Enquist and Card, 2003). Among these
54 tracer-based methods, the method based on engineered neurotropic viral vectors has made rapid and
55 substantial progress, particularly in mammals. Virus-based tracing is versatile as the target and spread
56 properties of the virus can be modified. Many virus species have been utilized and manipulated for this
57 purpose, such as rabies virus, vesicular stomatitis virus (VSV), herpes simplex virus (HSV), pseudorabies
58 virus (PRV), adeno-associated virus (AAV), retrovirus, lentivirus, canine adenovirus (CAV), semliki forest
59 virus, and Japanese encephalitis virus (Beier et al., 2011; Betley and Sternson, 2011; DeFalco et al., 2001;
60 Ekstrand et al., 2008; Jia et al., 2017; Jia et al., 2016; Kelly and Strick, 2000; Lo and Anderson, 2011;
61 Mazarakis et al., 2001; Salinas et al., 2009; Soudais et al., 2001; Ugolini, 2010; Wickersham et al., 2007),
62 *etc.* The viruses available for neuronal circuit dissection universally rely on the fluorescent signal, and the
63 detailed structures of the labeled neural cell bodies and fibers can clearly be viewed through fluorescent
64 imaging. However, it is difficult to longitudinally investigate the neural circuit spread over a large brain
65 area labeled for a given function or cell type using microscopic imaging.

66 On the other hand, as a non-invasive detection method, MRI has become an important tool for
67 understanding the brains of humans and animals. MRI can offer insights into the structure, function, and
68 metabolism of the brain (Rane et al., 2015), thus it has been widely used in scientific research and clinical
69 applications in recent years. With the help of relevant MRI approaches, such as DTI (Mori and Zhang,
70 2006), and Manganese-enhanced magnetic resonance imaging (MEMRI) (Lin and Koretsky, 1997; Pautler
71 et al., 1998; Silva et al., 2004), the neural networks can be predicted or detected. DTI-MRI produces
72 information of the axonal organization of the entire brain (Le Bihan, 2003), however, it cannot provide
73 information of anatomical connections through synapses. Mn^{2+} is anterogradely transported among
74 synaptic connections, enabling the revelation of brain connectivity (Koretsky, 2012; Tucciarone et al.,
75 2009; Zhang et al., 2010). Nevertheless, it is difficult to view the detailed structures of fibers and neurons
76 with MEMRI, due to the limited spatial resolution in MRI. Therefore, it is valuable to develop a novel
77 strategy that combines the advantages of neurotropic virus tracing and MRI approach.

78 As a metalloprotein (Cohen et al., 2007; Deans et al., 2006), ferritin is ubiquitous and highly
79 conserved throughout most organisms (Arosio et al., 2009). It has a paramagnetic effect after bonding with
80 iron in ferric (Fe^{3+}) forms (Owen and Lindsay, 1983) and a marked effect on solvent NMR relaxation rates
81 (Bulte et al., 1994; Gottesfeld and Neeman, 1996; Vymazal et al., 1998). Ferritin has been suggested as an
82 MRI reporter for the detection of gene expression using MRI in several studies (Cohen et al., 2005; Cohen
83 et al., 2007; Genove et al., 2005; Iordanova and Ahrens, 2012). Replication-defective adenovirus (AdV)
84 expressing ferritin can cause MRI contrast (T_2 and T_2^*) in the brain (Genove et al., 2005), and AdV
85 expressing a chimeric ferritin (light and heavy chain of ferritin fused by a linker, L*H) also enables the
86 visualization of endogenous neuroblast migration in the brain from the subventricular zone towards the

87 olfactory bulb (Iordanova and Ahrens, 2012). In a similar study, a lentiviral vector expressing ferritin was
88 utilized and ferritin-labeled endogenous neural stem cell progeny was detected with MRI (Vande Velde et
89 al., 2012). With lentiviral vector encoding ferritin and fluorescent proteins, tumors were detected by both
90 ferritin based MRI and fluorescence imaging methods (Kim et al., 2010). However, ferritin encoding virus
91 is rarely used to detect the neural connection. With the help of trans-synaptic neurotropic viruses and the
92 MRI method, ferritin could become a potential element to visualize synaptically connected networks.

93 In this study, ferritin was coupled to enhanced green fluorescent protein (EGFP) gene and cloned into
94 the VSV genome to generate a new trans-synaptic tracing tool. Our results demonstrate that the structural
95 neural connection can be detected with both MRI and fluorescent imaging. Thus, this study provides a
96 novel strategy which combines the methods of neurotropic virus tracing and MRI to visualize the labeled
97 global network for a given type or function in the brain, whose precise anatomical connections through
98 synapses can be verified through optical microimaging.

99

100 **2. Materials and Methods:**

101 **2.1 Animal experiments**

102 All animals involved in the experiments were treated in accordance with the protocols approved by
103 the Animal Ethics Committee at the Wuhan Institute of Physics and Mathematics, Chinese Academy of
104 Sciences (SYXK(E)2015-0051). All efforts were made to minimize animal suffering. Wild-type C57BL/6J
105 mice were obtained from Hunan SJA Laboratory Animal Co., Ltd (Hunan, China). All the mice were kept
106 in a 12h/12h light-dark cycle room (temperature, between 22-25 °C), and food and water were available *ad*
107 *libitum*.

108

109 **2.2 Virus construction**

110 Due to biosafety issues, the *in vivo* MRI scans could only be conducted with replication-restricted
111 rVSV-dG vectors, and the mice infected with rVSV vectors could not be used in the *in vivo* MRI study.
112 Thus, there were four different kinds of viral vectors developed in the current study. 1) rVSV-dG-EGFP
113 and rVSV-dG-Ferritin-EGFP: verify the virus expression of EGFP and detect the MRI signal of ferritin at
114 the injection site in the *in vivo* MRI study; 2) rVSV-EGFP and rVSV-Ferritin-EGFP: check the
115 trans-synaptic function of the viruses by optical imaging and detect the MRI signals of ferritin in multiple
116 brain regions postmortem.

117 **2.2.1 Plasmid construction**

118 The Ferritin-t2a-EGFP fragment was amplified from pLV-CAG-mFerritin-EGFP plasmid (a gift from
119 Prof. Xiaoming Li's lab in Zhejiang University). The chimeric ferritin gene (L*H) (from *Mus musculus*)
120 and EGFP gene were linked with a 2A self-cleavable sequence (GCGCGCGGC
121 GGCGGCGGCAGCGATTATAAAGATGATGATGATAAAGGCGGCGGCGGCAGCCGCGTG), the
122 fusion gene ((L*H)-t2a-EGFP fragment) was cloned into VSV vectors, rVSV-dG-EGFP (van den Pol et al.,
123 2009) (Fig. 1A) and rVSV-EGFP (pVSV-Venus-VSVG) (Beier et al., 2011) (Fig. 2A) respectively, using
124 XhoI and MscI cloning sites. In the virus genome, N, P, M, G and L are five VSV structural genes from a
125 wild type virus, and G was deleted to construct a replication-restricted recombinant virus, rVSV-dG. The
126 complete sequences of the recombinant constructs are shown in the supplementary materials.

127 **2.2.2 Virus production**

128 VSV viruses were rescued from plasmids as described in a previous study (Beier and Cepko, 2012).
129 For the production of rVSV-Ferritin-EGFP, three T75 bottles of BHK cells at 95% confluency were
130 infected at a MOI (multiplicity of infection) of 0.01. Viral supernatants were collected at 48 hpi. (hours

131 post-infection) and ultra-centrifuged (50,000 g) using a JA25.25 rotor (Beckman Coulter, USA) and
132 re-suspended with PBS in 0.1% of original volume. The concentrated viral stocks were titered in a dilution
133 series to 100% confluent BHK cells and EGFP plaques were examined at 12 hpi. For the production of
134 rVSV-dG-Ferritin-EGFP, 293T cells at 70% confluency on 10-cm dishes were transfected with 10 μ g of
135 pMD2.G (plasmid expressing VSVG) using FuGENE6 (Promega, USA). Twenty-four hours
136 post-transfection, the cells were infected at a MOI of 0.01 with rVSV-dG-Ferritin-EGFP. Viral supernatants
137 were collected at two dpi, then concentrated and the titer was determined as above. All viruses were stored
138 at -80 °C for subsequent experiments.

139

140 **2.3 Animal experiments**

141 2.3.1 Animal surgery

142 Eight-week-old male C57BL/6 mice (20–25 g) were injected with the virus. The procedures of virus
143 micro-injection are described in our previous study (Jia et al., 2016). Briefly, animals were anesthetized
144 with chloral hydrate (400 mg/Kg), and placed in a stereotaxic apparatus (Item: 68025 - stereotaxic
145 apparatus and 68030 - mice adaptor, RWD, China). The skull above the target area was thinned with a
146 dental drill and removed carefully. The injections were conducted with a 10 μ L syringe (Hamilton, Nevada,
147 USA) connected with a glass micropipette (10–15 μ m diameter tip). The virus (100 nL, titer: 2E8) was
148 stereotaxically microinjected into the target region. In order to minimize diffusion, syringes were kept in
149 place for 10 min after the injection was completed. The mice that were injected with rVSVs
150 (rVSV-Ferritin-EGFP, rVSV-EGFP, rVSV-dG-Ferritin-EGFP and rVSV-dG-EGFP) were kept in the
151 Biosafety Level 2 (BSL-2) laboratory animal room.

152 For the target regions, two brain sites were selected: CPU (Caudate Putamen) (0.02 mm anterior to
153 Bregma, 2 mm lateral from midline, 3 mm depth relative to Bregma) and SC (0.58 mm posterior to
154 Bregma, 1.5 mm lateral from midline, 1.15 mm depth relative to Bregma). The region CPU was used for
155 verifying the MRI contrast elicited by ferritin encoding VSV vector (rVSV-dG-Ferritin-EGFP) and
156 trans-multisynaptic characteristic of rVSV-Ferritin-EGFP; the other region SC was used to detect and
157 quantitatively analyze both the MRI and fluorescent signals of the trans-synaptic viruses
158 (rVSV-Ferritin-EGFP: FerritinEGFP group; rVSV-EGFP: EGFP group) in different infected regions.

159

160 2.3.2 Sample collection

161 The rVSV-Ferritin-EGFP and rVSV-EGFP viruses (both replication competent) must be handled
162 according to BSL-2 practices, which precluded use of the MRI scanner for imaging of live animals injected
163 with these viruses. These samples were therefore prepared for *ex vivo* imaging. To monitor the
164 virus-infected and iron loading procedures, the virus-infected mice were anaesthetized with an overdose of
165 chloral hydrate three or four days after injection. Then the animals were perfused with 0.9% saline solution
166 followed by 4% paraformaldehyde solution. The brain (with skull) was removed and imaged by the MRI
167 scanner using the protocol in the following section. After the MRI study, the brain was removed from the
168 skull and post-fixed over-night with 4% paraformaldehyde. The fixed brain was sectioned into 40 μ m
169 slices with a microtome (Leica, German). For Perls' Prussian Blue staining, the brain slices were immersed
170 in Perls' staining solution (Potassium ferrocyanide and hydrochloric acid - HCl, Solarbio, G1422, Beijing,
171 China) for 45 min and cell nuclei were counterstained with nuclear fast red. For immunohistochemistry
172 staining, the slices were incubated for 12 hours at 4°C with primary antibody (Abcam, ab69090, UK),
173 washed and incubated for 2 hours at 37°C with Cy3-labeled secondary antibody. For fluorescent imaging,
174 the brain slices were stained with DAPI and imaged by Olympus VS120 virtual microscopy slide scanning

175 system (Olympus, Japan) and confocal microscope (Leica SP8, German).

176

177 2.3.3 MRI

178 MRI images were acquired from the brains of mice in a horizontal-bore 7.0 T BioSpec machine
179 (Bruker, Ettlingen, Germany). A surface coil with a diameter of 20 mm was utilized in combination with a
180 birdcage transmit coil. Parameters included, the acquisition matrix size: 256×196 ; the reconstruction
181 matrix size: 256×256 ; field of view (FOV): $2.0 \text{ cm} \times 2.0 \text{ cm}$; and slice thickness: 0.5 mm. There were two
182 kinds of MRI studies involved, *in vivo* and *ex vivo*. The other acquisition parameters for these two methods
183 are respectively described as following:

184 For the *in vivo* MRI studies with living mice injected with rVSV-dG-Ferritin-EGFP and
185 rVSV-dG-EGFP, coronal slices were acquired at the injection site using T2-weighted spin-echo (Rapid
186 Acquisition with Relaxation Enhancement (RARE), TR/TE = 2,500/30-36ms, rare factor = 4, echo spacing
187 = 15-18 ms) and T2*-weighted gradient echo sequences (Fast Low Angle SHot (FLASH), TR/TE
188 = 500/15-16.5 ms, Flip angles=30°). As the contrast signals at the injection site were obviously observed,
189 the echo time (TE) was not optimized during the scanning of living animals. The average number for
190 T2-weighted imaging in living animals was set to 16, resulting in a total acquisition time of 32 min. The
191 average number for T2*-weighted imaging in living animals was set to 9, resulting in a total acquisition
192 time of 14 min. In order to avoid the motion artifacts during the scan, the animal was deeply anaesthetized,
193 and the concentration of isoflurane was adjusted to 1.0-1.5%. The breath rate was controlled under 60
194 times/min. A warm water pad was utilized to maintain the body temperature of the animals (~37°C).

195 According to the biological safety requirements for VSV, the living mice infected with
196 rVSV-Ferritin-EGFP or rVSV-EGFP must not be directly scanned using the MRI scanner. Thus, the
197 virus-infected mice were perfused, and the brain (with skull) removed for the *ex vivo* MRI study. The *ex*
198 *in vivo* MRI scans for the intact brain were acquired using T2-weighted spin-echo sequence, and the average
199 number was set to 16, resulting in the total acquisition time of 39 min. In order to improve the image
200 quality for quantitative analysis, the parameters were optimized to TR/TE = 3,000/50ms (RARE, rare
201 factor = 4, echo spacing = 25 ms) for better T2 contrast and image quality.

202

203 2.4 Data Processing

204 The procedures of analysis for fluorescence imaging and MRI are described separately:

205 For fluorescent images, the fluorescent signals in a given slice were automatically co-registered to the
206 mice Allen brain atlas with a recently developed software (Agarwal et al., 2018), so as to reveal the
207 locations of the fluorescent signals. In their method, 20 different ROIs were automatically recognized
208 without distinguishing the left and right hemispheres. Thus, this ROI recognition method was not suitable
209 for our work. In order to analyze the relationship between the MRI and fluorescent signals in different
210 ROIs, the virus infected regions were manually traced out after the alignment of fluorescent images and
211 brain atlas, and EGFP fluorescent signal intensities in the ROIs were extracted. Since all the optical
212 imaging parameters were set the same and the green channel of the images were not overexposed, the
213 green fluorescent signals were normalized using the highest value in all images.

214 For the *in vivo* MRI study, the rVSV-dG-Ferritin-EGFP infected area in the mice brain was manually
215 drawn with Paravision 5.0 (Bruker Biospec, Germany), and the symmetrical site in the contralateral side
216 was marked, then the MRI signals on both sides were collected for comparison. The MRI signal intensity
217 of cerebrospinal fluid (CSF) in each animal was extracted and used as the reference to normalize the MRI
218 signal intensity. (O'Neill et al., 2002; Tjoa et al., 2005).

219 For the *ex vivo* MRI study, the raw data was converted to nifti (hdr/img) format using
220 Bruker2Analyze Converter (<http://people.cas.sc.edu/rorden/micro/bru2anz/>). The ferritin-expressing areas
221 were segmented based on mouse brain MRI-T2 templates and atlas images. The atlas images of the mouse
222 brain were constructed from the Paxinos and Franklin atlas figures, as described in our previous study (Nie
223 et al., 2018). First, every individual image of the mouse brain was co-registered with a pair of brain
224 template and brain atlas images, using the nearest interpolation method (Nie et al., 2013). Next, the
225 spreading areas of ferritin encoding virus were identified by considering both the fluorescent signals and
226 the difference between MRI signals in EGFP and FerritinEGFP groups, and the spreading areas of each
227 mouse were manually traced out using MRIcron (<https://www.nitrc.org/projects/mricron>) and saved as a
228 mask image. Then, the overlapping voxels between the mask image and registered atlas image were
229 determined. According to the sub-anatomical regional index in the atlas image, the spreading area of the
230 ferritin encoding virus was segmented into several sub-anatomical regions. Finally, the mean voxel
231 intensity in each sub-anatomical region was automatically calculated and normalized with MRI signal
232 intensity in CSF. The following ROI were analyzed: Auditory cortex (AuC)_right (R), Caudate Putamen
233 (CPU)_Left (L), CPU_R, Hippocampus (Hipp)_L, Hipp_R, Motor Cortex (MC)_L, MC_R, Retrosplenial
234 cortex (RSC)_R, Somatosensory Cortex (SC)_L, SC_R, Thalamus (TH)_R, Visual Cortex (ViC)_R.

235 All of the data processing and analyses were implemented in MATLAB (MathWorks, Inc., USA).

236 237 **2.5 Statistical analysis**

238 All MRI signals were normalized with MRI signal intensity in cerebrospinal fluid (CSF). For
239 comparison of the MRI signals in animals infected with rVSV-dG-EGFP and rVSV-dG-Ferritin-EGFP, a
240 paired *t*-test was applied; the MRI signal and fluorescent signal intensities in the FerritinEGFP and EGFP
241 groups were compared with an independent student *t*-test (Two-tailed, $P < 0.05$). Results were presented in
242 Average \pm Standard deviation (Ave. \pm STD).

243 244 245 **3. Results**

246 **3.1 Effect of ferritin expressed by non-trans-synaptic VSV on MRI signal in living animals**

247 Seven days after rVSV-dG-Ferritin-EGFP and the control virus (rVSV-dG-EGFP) were
248 stereotactically microinjected into the right and left sides of CPU, respectively (Fig. 1A, $n = 6$), MRI
249 studies were conducted in the living animals. The right injection site showed a robust contrast in both T2-
250 and T2*-weighted images (Fig. 1B and 1C), while the left side did not. The fluorescent image of the same
251 brain slice is shown in Fig. 1D, and it illustrates that the expression of the green fluorescence in the two
252 injection sites are similar. The T2 and T2* weighted MRI signals were normalized with MRI signal
253 intensity in CSF for comparison across subjects. The statistical results show that the brain region infected
254 with rVSV-dG-Ferritin-EGFP had significantly reduced T2 (Fig. 1E, $p < 0.05$) and T2* (Fig. 1F, $p < 0.01$)
255 weighted MRI signals. The results verified that ferritin expressed by rVSV-dG-Ferritin-EGFP could be
256 used as an MRI contrast agent.

257 258 **3.2 Trans-multi-synaptic property of rVSV-Ferritin-EGFP**

259 The Ferritin-EGFP fused gene was cloned into a trans-multisynaptic tracing VSV system to construct
260 a new recombinant virus, rVSV-Ferritin-EGFP (Fig. 2A), which probably spreads anterogradely along
261 synaptic connections as rVSV-EGFP (Beier et al., 2011). rVSV-Ferritin-EGFP was stereotactically
262 microinjected into CPU (Fig. 2B, $n = 2$). The mice were perfused and decapitated for MRI scanning and

263 fluorescent imaging four days post-injection. The EGFP signals were detected in several regions including
264 the injection site (Fig. 2C & Fig. S1). Among these regions, the substantia nigra (SN) and TH have been
265 reported to be the primary and secondary anterograde targets of CPU, respectively (Fig. 2D and 2E)
266 (Keeler et al., 2014). The results of fluorescent imaging show that the rVSV-Ferritin-EGFP could be
267 utilized as an anterograde trans-multi-synaptic vector similar to rVSV-EGFP (Beier et al., 2011).

268 Changes of MRI T2 contrast were observed in CPU and SN (Fig. S2), but not in TH. This might be
269 caused by multi-synapse connection between TH and CPU, and ferritin expressed by the virus in TH not
270 having enough time to enrich Fe^{3+} . Furthermore, the location of TH was further away from the surface coil
271 compared with SN (The surface coil was located at the bottom of the head). In order to obtain better
272 imaging quality and verify this novel strategy, first, another cortical region, SC, was selected in the
273 following studies, and the surface coil was located dorsal to the brain (close to mouse cerebral cortex).

274

275 **3.3 Detection of neural connections with ex vivo MRI and fluorescent imaging**

276 Both trans-multi-synaptic virus tracers, rVSV-Ferritin-EGFP and rVSV-EGFP, were stereotactically
277 microinjected into SC in two separated mice groups (n = 5 for each group) for both MRI and fluorescent
278 imaging.

279 At first, three days after the injection, the mice were perfused and the brains (with skull) were
280 subjected to the MRI scanner. There was overt T2 weighted MRI contrast in the local injection site, and
281 only a few other brain regions seemed to show MRI contrast (Fig. S3), while green fluorescent signals
282 were observed in many regions. Thus, the iron accumulation could be one of the important factors that
283 influenced the MRI contrast.

284 Due to the cyto-toxicity of the replication complete VSV involved here (rVSV-EGFP and
285 rVSV-Ferritin-EGFP), the infected animals died about four and a half days after the virus injection. So we
286 chose to sacrifice the animals four days post-injection. Four days after the injection, the T2-weighted MRI
287 images showed robust contrast in several brain regions in the FerritinEGFP group (rVSV-Ferritin-EGFP
288 injected), while no discernable T2 contrast was found in the EGFP group (rVSV-EGFP injected) (Fig. 3).
289 The darker MRI signal around the injection site in the EGFP group might be caused by tissue damage
290 during the virus microinjection procedure. The high-resolution images of the registration results of the
291 fluorescent images and Allen Mouse Brain Connectivity Atlas (connectivity.brain-map.org) are provided in
292 the supplemental material. (Fig. S4). The fluorescent images show that the green fluorescent signals were
293 mainly distributed into 12 different brain regions - AuC_R, CPU_L, CPU_R, Hipp_L, Hipp_R, MC_L,
294 MC_R, RSC_R, SC_L, SC_R, TH_R, ViC_R. These results also demonstrate that rVSV-EGFP and
295 rVSV-Ferritin-EGFP mainly spread into the same brain regions.

296 Comparing the fluorescent and MRI images in the FerritinEGFP group, there is an extensive overlap
297 between MRI contrast and EGFP signals in the virus infected brain regions. These results confirm that the
298 MRI contrast in the T2-weighted image caused by ferritin in the rVSV-Ferritin-EGFP is detectable and
299 traceable.

300

301 **3.4 Comparing the results of MRI signals in FerritinEGFP and EGFP groups**

302 In order to quantitatively analyze the MRI contrast caused by ferritin in the rVSV-Ferritin-EGFP, the
303 normalized MRI signals between the FerritinEGFP and EGFP groups were compared. The MRI signals of
304 12 brain regions that displayed obvious fluorescent signals in both groups were collected (Fig. 4). There
305 was no virus infection in the Olfactory tubercle_R (OT_R) and OT_L, thus they were selected as control.

306 The T2-weighted MRI signals in the FerritinEGFP group were significantly lower (Fig. 4B, $p < 0.01$),

307 which indicates that there was neuronal connectivity between these 11 virus-spreading brain regions and
308 the virus injection site (SC_R). Due to the properties of the virus, these regions could be synaptically
309 connected downstream regions of the SC_R. These results reveal that the rVSV-Ferritin-EGFP could be
310 utilized as a trans-multi-synaptic neural circuit tracer using *ex vivo* MRI and fluorescent imaging
311 approaches.

312

313 **3.5 Immunohistochemistry and Perls' Prussian Blue staining**

314 Immunohistochemistry was performed to detect ferritin expression and verify the co-localization of
315 ferritin and EGFP. In the FerritinEGFP group, the ferritin and EGFP showed similar expression patterns
316 and considerable signal overlaps in virus infected neurons (Fig. 5 & 6). Ferritin could cause the MRI
317 contrast *via* the iron loading in its protein cage. In the FerritinEGFP group, Perls' Prussian Blue staining
318 for iron (arrows) with Nuclear fast red counterstaining revealed the presence of Fe^{3+} in several brain
319 regions (SC, CPU, Hipp, ViC and TH), in which all showed hypointense contrast in MRI images (Fig.
320 7A-H). OT was selected as the control region for comparison (Fig. 7I), where MRI signal was not
321 significantly changed. There was lack of obvious Perls' Prussian Blue staining positive signal in OT.
322 Furthermore, there was no overt iron accumulation in the control group (data not shown).

323

324 **3.6 The relationship of MRI and fluorescent imaging signal intensities**

325 In order to measure the efficiency of the MRI method for detecting the neural connections, the
326 relationship of MRI contrast and green fluorescent signal intensity in the FerritinEGFP group was analyzed.
327 Because the neural connections with contralateral brain regions are more complicated, the injection site
328 (SC_R) and seven ipsilateral brain regions with significant MRI contrast were included for the analysis of
329 the correlation between MRI and fluorescent signals. Among these eight brain regions, the relationship
330 between the green fluorescent signal intensity in the FerritinEGFP group and the ratio of the difference in
331 normalized MRI signal intensities between groups (EGFP and FerritinEGFP) and the normalized MRI
332 signal intensities in the EGFP group ($(S_{EGFP} - S_{FerritinEGFP}) / S_{EGFP}$, 'S' represents normalized MRI signal
333 intensity) is illustrated (Fig. 8). According to the information in the Allen Mouse Brain Connectivity Atlas
334 (connectivity.brain-map.org), all regions in Fig. 8 except Hipp_R receive direct projections from SC_R,
335 which means that they are directly connected to the injection site. Thus, the time to accumulate iron in
336 Hipp_R is different from other regions, which results in different MRI contrast. Therefore, linear
337 regression analysis was applied for the rest six brain regions, $y = 0.4494x + 0.1302$ ($R^2 = 0.5904$). Besides,
338 there was no significant difference in the fluorescent signal intensities of the selected ROIs in the groups of
339 FerritinEGFP and EGFP (Fig. S5).

340

341 **4. Discussion**

342 Neural circuits are both extremely complex and exquisitely specific. Currently, neurotropic viral tracing is
343 one of the most popular methods in neural circuitry exploration. Mostly, neurotropic viral tracers are
344 viewed with microscopy imaging, which is not suitable for longitudinal investigation of the neural circuit.
345 Here, our results demonstrate that structural neural connections could be detected using both *ex vivo* MRI
346 and fluorescent imaging with the help of ferritin-EGFP fused gene encoding neurotropic viruses. The
347 current strategy has the potential application of longitudinal monitoring of neural circuits in living animals.
348 However, a few caveats, solutions and perspectives need to be discussed.

349

350 **4.1 Explanation of T2 hypointense contrast caused by Ferritin encoding virus**

351 The optical measurement is mostly influenced by the expression level of EGFP. However, multiple
352 confounding factors affect the ferritin-based MRI signal. The signal could be influenced by cellular iron
353 loading, which is determined by a few factors, including the level of ferritin expressed in the infected
354 neurons, the iron enrichment capability of the infected neurons, the availability of iron ions, and the
355 duration of the enrichment period. Other factors related to imaging signals include the distance between
356 the infected regions and the surface coil, and the state of the imaging system such as shimming quality.

357 It is difficult to optimize all these experimental parameters to quantitatively resolve explicit
358 relationships between the MRI signals and the ferritin encoding trans-synaptic virus infection in different
359 brain regions. There were eight ipsilateral virus infected brain regions involved in the current study (Fig. 8).
360 The injection site, SC_R, showed the highest EGFP fluorescent signal intensity, unlike its MRI contrast.
361 This could be caused by the operation damage and inflammation at the injection site of both groups. The
362 region Hipp_R is not directly connected to the injection site – SC_R, and there was less time for the
363 ferritin expressed in Hipp_R to enrich iron, thus, the difference of MRI signal intensity may be
364 correspondingly weak. Among the rest of the regions, the difference in normalized MRI signal intensity
365 increased following the rise of green fluorescent signal intensity, which indicates that more ferritin-EGFP
366 expressed in the virus infected neurons resulted in stronger MRI contrast. Anyway, more efforts to
367 elucidate the complex relationship between the MRI signals and ferritin encoding trans-synaptic virus
368 infection is ongoing.

369 **4.2 Application of other kinds of MRI reporters**

371 In the current study, ferritin was cloned into VSV to generate a modified virus in order to investigate
372 the neural connections in the brain. Other kinds of MRI reporter genes could be delivered by trans-synaptic
373 viruses for neural circuit tracing systems. Currently, there are a number of MRI reporters (Kang and Chung,
374 2008; Mukherjee et al., 2016; Ray et al., 2003; Weissleder et al., 1997), such as transferrin receptor (Kang
375 and Chung, 2008; Weissleder et al., 2000), beta-galactosidase (Louie et al., 2000), MagA (Zurkiya et al.,
376 2008), Tyrosinase (Alfke et al., 2003; Weissleder et al., 1997), LRP (Gilad et al., 2007), and human
377 aquaporin 1(AQP1) (Mukherjee et al., 2016). These modified tools could be detected using different kinds
378 of MRI methods, such as T2 and T2* (transferrin receptor, beta-galactosidase and MagA), T1 (Tyrosinase),
379 CEST (Chemical Exchange Saturation Transfer: LRP), or DWI (AQP1).

380 **4.3 Limitation and Perspective**

382 According to the biological safety requirements of VSV, this related *in vivo* study should be
383 conducted in the BSL-2 laboratory, and the living mice infected with rVSV cannot be directly scanned
384 using the MRI scanner. Thus, the virus-infected mice were perfused, and the brain (with skull) was
385 removed for *ex vivo* MRI study. However, this study provided a novel concept to directly detect the neural
386 connection using MRI method, and it also has a potential ability to longitudinally trace the neural circuit.

387 There are different strategies to overcome the limitation that *in vivo* MRI study is not allowed for
388 rVSV infected mice. It is possible to construct a micro-isolation system that satisfies the BSL-2
389 environment and is compatible with MRI scanner for *in vivo* MRI imaging of VSV infected mice in future
390 study. With the help of the system, the virus infected mice would be continuously scanned at different
391 intervals post injection in a longitudinal study.

392 A more attractive alternative is to develop new toxicity attenuated viruses which could be used to
393 trace neural circuits in live animals using a normal MRI scanner. In the current study, VSV was utilized to
394 label the neurons at the injection site and the multi-step outputs from the starting area, as it spread

395 exclusively anterogradely in neural circuit (Beier et al., 2011). With the help of other kinds of ferritin
396 encoding neurotropic viruses, the neural circuitry with different spread directions or cascade of synaptic
397 connections could be dissected. If ferritin is cloned into this monosynaptic labeling system, the direct
398 output of the type-specific start neurons might be detected by the MRI T2-weighted image. Using a similar
399 method, the PRV system carrying ferritin could provide the input of the starting neurons with MRI.
400 Furthermore, CAV or rAAV2-retro with ferritin could map the direct input of the start neurons using the
401 same approach (Soudais et al., 2001; Tervo et al., 2016). Development of a new tracing system and toxicity
402 attenuation of VSV, PRV and HSV have been included in ongoing projects in the laboratory.

403 In the future, with the development of attenuated virus, which is a challenge when detecting neural
404 circuit in live animals, the neural circuit could be observed longitudinally. During future live animal
405 studies, the MRI detection conditions could be similar to the method used in Fig. 1. The MRI scanning
406 parameters such as repetition time and echo time could be optimized for better signal noise ratio and T2
407 contrast. Therefore, this approach has the potential application to longitudinally trace the neural circuit in
408 live animals.

409

410 5. Conclusion

411 To summarize, the advantages of neurotropic virus based neural circuit tracing and MRI technology
412 were combined together in this new strategy, which enabled the detection of the neural connection using
413 both *ex vivo* MRI and fluorescent imaging. The MRI reporter gene ferritin was cloned into the VSV system
414 and sufficiently elicited MRI contrast in the T2-weighted image. After the virus injection, propagation and
415 trans-synaptic transmission, MRI contrasts and EGFP signals were observed in the same brain regions.
416 This method exhibits the neural connection through MRI detection and allows high-resolution microscopy
417 detection of fine structures in neural pathways, which bridge the observation of neural connections from
418 macroscopic and microscopic scales. The strategy of the current study has the potential to investigate
419 neural circuits in live animals.

420

421 Acknowledgement

422 The authors would like to express their gratitude to Graeme F. Mason (Yale University, USA) for the
423 help of discussion and manuscript writing; Mr. Hansen Wu (Vanderbilt University, USA) and Bruno
424 Hamish Unger (University of Otago, New Zealand) for the proofreading; Dr. Nitin Agarwal (University of
425 California) for providing the program (Agarwal et al., 2018) for registration of fluorescent images and
426 mice brain atlas; Dr. Zhengwu Zhang (University of Rochester) for performing the fluorescent image
427 registration.

428

429 **Funding:** This work was supported by the Chinese Ministry of Science and Technology (2015CB755601,
430 2015AA020508); the Chinese Academy of Science (XDB02050005); and the National Natural Science
431 Foundation of China (31400976) and the Youth Innovation Promotion Association of Chinese Academy of
432 Sciences (Y6Y0021004).

433

434 Financial Disclosures

435 The authors report no biomedical financial interests or potential conflicts of interest.

436

437 Reference:

438 Agarwal, N., Xu, X., Gopi, M., 2018. Geometry processing of conventionally produced mouse brain slice images.

- 439 Journal of Neuroscience Methods 306, 45-56.
- 440 Alfke, H., Stöppler, H., Nocken, F., Heverhagen, J.T., Kleb, B., Czubayko, F., Klose, K.J., 2003. In Vitro MR Imaging
441 of Regulated Gene Expression. *Radiology* 228, 488-492.
- 442 Arosio, P., Ingrassia, R., Cavadini, P., 2009. Ferritins: a family of molecules for iron storage, antioxidation and
443 more. *Biochim Biophys Acta* 1790, 589-599.
- 444 Beier, K., Cepko, C., 2012. Viral Tracing of Genetically Defined Neural Circuitry. *Jove-Journal of Visualized*
445 *Experiments*.
- 446 Beier, K.T., Saunders, A., Oldenburg, I.A., Miyamichi, K., Akhtar, N., Luo, L., Whelan, S.P., Sabatini, B., Cepko, C.L.,
447 2011. Anterograde or retrograde transsynaptic labeling of CNS neurons with vesicular stomatitis virus vectors.
448 *Proc Natl Acad Sci U S A* 108, 15414-15419.
- 449 Betley, J.N., Sternson, S.M., 2011. Adeno-associated viral vectors for mapping, monitoring, and manipulating
450 neural circuits. *Hum Gene Ther* 22, 669-677.
- 451 Brog, J.S., Salyapongse, A., Deutch, A.Y., Zahm, D.S., 1993. The Patterns of Afferent Innervation of the Core and
452 Shell in the Accumbens Part of the Rat Ventral Striatum - Immunohistochemical Detection of Retrogradely
453 Transported Fluorogold. *Journal of Comparative Neurology* 338, 255-278.
- 454 Bulte, J.W.M., Douglas, T., Mann, S., Frankel, R.B., Moskowitz, B.M., Brooks, R.A., Baumgarner, C.D., Vymazal, J.,
455 Strub, M.P., Frank, J.A., 1994. Magnetoferritin - Characterization of a Novel Superparamagnetic Mr Contrast
456 Agent. *Journal of Magnetic Resonance Imaging* 4, 497-505.
- 457 Callaway, E.M., 2008. Transneuronal circuit tracing with neurotropic viruses. *Current Opinion in Neurobiology*
458 18, 617-623.
- 459 Cohen, B., Dafni, H., Meir, G., Harmelin, A., Neeman, M., 2005. Ferritin as an endogenous MRI reporter for
460 noninvasive imaging of gene expression in C6 glioma tumors. *Neoplasia* 7, 109-117.
- 461 Cohen, B., Ziv, K., Plaks, V., Israely, T., Kalchenko, V., Harmelin, A., Benjamin, L.E., Neeman, M., 2007. MRI
462 detection of transcriptional regulation of gene expression in transgenic mice. *Nature Medicine* 13, 498-503.
- 463 Deans, A.E., Wadghiri, Y.Z., Bernas, L.M., Yu, X., Rutt, B.K., Turnbull, D.H., 2006. Cellular MRI contrast via
464 coexpression of transferrin receptor and ferritin. *Magn Reson Med* 56, 51-59.
- 465 DeFalco, J., Tomishima, M., Liu, H., Zhao, C., Cai, X., Marth, J.D., Enquist, L., Friedman, J.M., 2001. Virus-assisted
466 mapping of neural inputs to a feeding center in the hypothalamus. *Science* 291, 2608-2613.
- 467 Ekstrand, M.I., Enquist, L.W., Pomeranz, L.E., 2008. The alpha-herpesviruses: molecular pathfinders in nervous
468 system circuits. *Trends Mol Med* 14, 134-140.
- 469 Enquist, L.W., Card, J.P., 2003. Recent advances in the use of neurotropic viruses for circuit analysis. *Current*
470 *Opinion in Neurobiology* 13, 603-606.
- 471 Genove, G., DeMarco, U., Xu, H., Goins, W.F., Ahrens, E.T., 2005. A new transgene reporter for in vivo magnetic
472 resonance imaging. *Nat Med* 11, 450-454.
- 473 Gilad, A.A., McMahon, M.T., Walczak, P., Winnard, P.T., Raman, V., van Laarhoven, H.W.M., Skoglund, C.M., Bulte,
474 J.W.M., van Zijl, P.C.M., 2007. Artificial reporter gene providing MRI contrast based on proton exchange. *Nature*
475 *Biotechnology* 25, 217-219.
- 476 Gottesfeld, Z., Neeman, M., 1996. Ferritin effect on the transverse relaxation of water: NMR microscopy at 9.4 T.
477 *Magnetic Resonance in Medicine* 35, 514-520.
- 478 Horowitz, L.F., Montmayeur, J.P., Echelard, Y., Buck, L.B., 1999. A genetic approach to trace neural circuits.
479 *Proceedings of the National Academy of Sciences of the United States of America* 96, 3194-3199.
- 480 Iordanova, B., Ahrens, E.T., 2012. In vivo magnetic resonance imaging of ferritin-based reporter visualizes native
481 neuroblast migration. *NeuroImage* 59, 1004-1012.
- 482 Jia, F., Miao, H., Zhu, X.T., Xu, F.Q., 2017. Pseudo-typed Semliki Forest virus delivers EGFP into neurons. *Journal*

- 483 of Neurovirology 23, 205-215.
- 484 Jia, F., Zhu, X., Xu, F., 2016. A single adaptive point mutation in Japanese encephalitis virus capsid is sufficient to
485 render the virus as a stable vector for gene delivery. *Virology* 490, 109-118.
- 486 Kang, J.H., Chung, J.K., 2008. Molecular-genetic imaging based on reporter gene expression. *Journal of Nuclear*
487 *Medicine* 49, 164s-179s.
- 488 Keeler, J.F., Pretsell, D.O., Robbins, T.W., 2014. Functional implications of dopamine D1 vs. D2 receptors: A
489 'prepare and select' model of the striatal direct vs. indirect pathways. *Neuroscience* 282, 156-175.
- 490 Kelly, R.M., Strick, P.L., 2000. Rabies as a transneuronal tracer of circuits in the central nervous system. *J*
491 *Neurosci Methods* 103, 63-71.
- 492 Kim, H.S., Cho, H.R., Choi, S.H., Woo, J.S., Moon, W.K., 2010. In vivo Imaging of Tumor Transduced with Bimodal
493 Lentiviral Vector Encoding Human Ferritin and Green Fluorescent Protein on a 1.5T Clinical Magnetic
494 Resonance Scanner. *Cancer Research* 70, 7315-7324.
- 495 Koretsky, A.P., 2012. Is there a path beyond BOLD? Molecular imaging of brain function. *NeuroImage* 62,
496 1208-1215.
- 497 Lai, B.Q., Qiu, X.C., Zhang, K., Zhang, R.Y., Jin, H., Li, G., Shen, H.Y., Wu, J.L., Ling, E.A., Zeng, Y.S., 2015. Cholera
498 Toxin B Subunit Shows Transneuronal Tracing after Injection in an Injured Sciatic Nerve. *Plos One* 10.
- 499 Le Bihan, D., 2003. Looking into the functional architecture of the brain with diffusion MRI. *Nature Reviews*
500 *Neuroscience* 4, 469-480.
- 501 Lerner, T.N., Ye, L., Deisseroth, K., 2016. Communication in Neural Circuits: Tools, Opportunities, and Challenges.
502 *Cell* 164, 1136-1150.
- 503 Lin, Y.J., Koretsky, A.P., 1997. Manganese ion enhances T1-weighted MRI during brain activation: an approach
504 to direct imaging of brain function. *Magn Reson Med* 38, 378-388.
- 505 Lo, L., Anderson, D.J., 2011. A Cre-dependent, anterograde transsynaptic viral tracer for mapping output
506 pathways of genetically marked neurons. *Neuron* 72, 938-950.
- 507 Louie, A.Y., Huber, M.M., Ahrens, E.T., Rothbacher, U., Moats, R., Jacobs, R.E., Fraser, S.E., Meade, T.J., 2000. In
508 vivo visualization of gene expression using magnetic resonance imaging. *Nat Biotech* 18, 321-325.
- 509 Mazarakis, N.D., Azzouz, M., Rohll, J.B., Ellard, F.M., Wilkes, F.J., Olsen, A.L., Carter, E.E., Barber, R.D., Baban, D.F.,
510 Kingsman, S.M., Kingsman, A.J., O'Malley, K., Mitrophanous, K.A., 2001. Rabies virus glycoprotein pseudotyping
511 of lentiviral vectors enables retrograde axonal transport and access to the nervous system after peripheral
512 delivery. *Hum Mol Genet* 10, 2109-2121.
- 513 Mori, S., Zhang, J., 2006. Principles of diffusion tensor imaging and its applications to basic neuroscience
514 research. *Neuron* 51, 527-539.
- 515 Mukherjee, A., Wu, D., Davis, H.C., Shapiro, M.G., 2016. Non-invasive imaging using reporter genes altering
516 cellular water permeability. *Nature Communications* 7.
- 517 Nie, B., Chen, K., Zhao, S., Liu, J., Gu, X., Yao, Q., Hui, J., Zhang, Z., Teng, G., Zhao, C., Shan, B., 2013. A rat brain
518 MRI template with digital stereotaxic atlas of fine anatomical delineations in paxinos space and its automated
519 application in voxel-wise analysis. *Human Brain Mapping* 34, 1306-1318.
- 520 Nie, B., Wu, D., Liang, S., Liu, H., Sun, X., Li, P., Huang, Q., Zhang, T., Feng, T., Ye, S., Zhang, Z., Shan, B., 2018. A
521 stereotaxic MRI template set of mouse brain with fine sub-anatomical delineations: Application to MEMRI
522 studies of 5XFAD mice. *Magn Reson Imaging* 57, 83-94.
- 523 Numan, M., Numan, M.J., 1997. Projection sites of medial preoptic area and ventral bed nucleus of the stria
524 terminalis neurons that express Fos during maternal behavior in female rats. *Journal of Neuroendocrinology* 9,
525 369-384.
- 526 O'Neill, J., Schuff, N., Marks, W.J., Feiwell, R., Aminoff, M.J., Weiner, M.W., 2002. Quantitative H-1 magnetic

- 527 resonance spectroscopy and MRI of Parkinson's disease. *Movement Disorders* 17, 917-927.
- 528 Owen, C.S., Lindsay, J.G., 1983. Ferritin as a Label for High-Gradient Magnetic Separation. *Biophysical Journal*
- 529 42, 145-150.
- 530 Paton, J.A., Nottebohm, F., 1984. Neurons Generated in the Adult Brain Are Recruited into Functional Circuits.
- 531 *Science* 225, 1046-1048.
- 532 Pautler, R.G., Silva, A.C., Koretsky, A.P., 1998. In vivo neuronal tract tracing using manganese-enhanced
- 533 magnetic resonance imaging. *Magn Reson Med* 40, 740-748.
- 534 Rane, P., Cochran, D., Hodge, S.M., Haselgrove, C., Kennedy, D.N., Frazier, J.A., 2015. Connectivity in Autism: A
- 535 Review of MRI Connectivity Studies. *Harvard Review of Psychiatry* 23, 223-244.
- 536 Ray, P., Wu, A.M., Gambhir, S.S., 2003. Optical bioluminescence and positron emission tomography imaging of a
- 537 novel fusion reporter gene in tumor xenografts of living mice. *Cancer Research* 63, 1160-1165.
- 538 Salinas, S., Bilsland, L.G., Henaff, D., Weston, A.E., Keriell, A., Schiavo, G., Kremer, E.J., 2009. CAR-associated
- 539 vesicular transport of an adenovirus in motor neuron axons. *PLoS Pathog* 5, e1000442.
- 540 Silva, A.C., Lee, J.H., Aoki, I., Koretsky, A.P., 2004. Manganese-enhanced magnetic resonance imaging (MEMRI):
- 541 methodological and practical considerations. *NMR Biomed* 17, 532-543.
- 542 Soudais, C., Laplace-Builhe, C., Kissa, K., Kremer, E.J., 2001. Preferential transduction of neurons by canine
- 543 adenovirus vectors and their efficient retrograde transport in vivo. *FASEB Journal* 15, 2283-2285.
- 544 Tervo, D.G., Hwang, B.Y., Viswanathan, S., Gaj, T., Lavzin, M., Ritola, K.D., Lindo, S., Michael, S., Kuleshova, E.,
- 545 Ojala, D., Huang, C.C., Gerfen, C.R., Schiller, J., Dudman, J.T., Hantman, A.W., Looger, L.L., Schaffer, D.V., Karpova,
- 546 A.Y., 2016. A Designer AAV Variant Permits Efficient Retrograde Access to Projection Neurons. *Neuron* 92,
- 547 372-382.
- 548 Tjoa, C.W., Benedict, R.H.B., Weinstock-Guttman, B., Fabiano, A.J., Bakshi, R., 2005. MRI T2 hypointensity of the
- 549 dentate nucleus is related to ambulatory impairment in multiple sclerosis. *Journal of the Neurological Sciences*
- 550 234, 17-24.
- 551 Tucciarone, J., Chuang, K.H., Dodd, S.J., Silva, A., Pelled, G., Koretsky, A.P., 2009. Layer specific tracing of
- 552 corticocortical and thalamocortical connectivity in the rodent using manganese enhanced MRI. *NeuroImage* 44,
- 553 923-931.
- 554 Tye, K.M., Deisseroth, K., 2012. Optogenetic investigation of neural circuits underlying brain disease in animal
- 555 models. *Nature Reviews: Neuroscience* 13, 251-266.
- 556 Ugolini, G., 2010. Advances in viral transneuronal tracing. *J Neurosci Methods* 194, 2-20.
- 557 van den Pol, A.N., Ozduman, K., Wollmann, G., Ho, W.S., Simon, I., Yao, Y., Rose, J.K., Ghosh, P., 2009. Viral
- 558 strategies for studying the brain, including a replication-restricted self-amplifying delta-G vesicular stomatis
- 559 virus that rapidly expresses transgenes in brain and can generate a multicolor golgi-like expression. *J Comp*
- 560 *Neurol* 516, 456-481.
- 561 Vande Velde, G., Raman Rangarajan, J., Vreys, R., Guglielmetti, C., Dresselaers, T., Verhoye, M., Van der Linden,
- 562 A., Debyser, Z., Baekelandt, V., Maes, F., Himmelreich, U., 2012. Quantitative evaluation of MRI-based tracking
- 563 of ferritin-labeled endogenous neural stem cell progeny in rodent brain. *Neuroimage* 62, 367-380.
- 564 Vymazal, J., Brooks, R.A., Bulte, J.W.M., Gordon, D., Aisen, P., 1998. Iron uptake by ferritin: NMR relaxometry
- 565 studies at low iron loads. *Journal of Inorganic Biochemistry* 71, 153-157.
- 566 Weissleder, R., Moore, A., Mahmood, U., Bhorade, R., Benveniste, H., Chiocca, E.A., Basilion, J.P., 2000. In vivo
- 567 magnetic resonance imaging of transgene expression. *Nat Med* 6, 351-355.
- 568 Weissleder, R., Simonova, M., Bogdanova, A., Bredow, S., Enochs, W.S., Bogdanov, A., 1997. MR imaging and
- 569 scintigraphy of gene expression through melanin induction. *Radiology* 204, 425-429.
- 570 Wickersham, I.R., Lyon, D.C., Barnard, R.J., Mori, T., Finke, S., Conzelmann, K.K., Young, J.A., Callaway, E.M.,

- 571 2007. Monosynaptic restriction of transsynaptic tracing from single, genetically targeted neurons. *Neuron* 53,
572 639-647.
- 573 Zhang, X.W., Bearer, E.L., Boulat, B., Hall, F.S., Uhl, G.R., Jacobs, R.E., 2010. Altered Neurocircuitry in the
574 Dopamine Transporter Knockout Mouse Brain. *PLoS One* 5.
- 575 Zurkiya, O., Chan, A.W., Hu, X., 2008. MagA is sufficient for producing magnetic nanoparticles in mammalian
576 cells, making it an MRI reporter. *Magn Reson Med* 59, 1225-1231.
- 577

ACCEPTED MANUSCRIPT

578 **Figure Legends**

579 Fig. 1. Detection of ferritin delivered by replication-defective VSV with MRI in living animals (n=6). *Note:*
 580 *A: Virus genomes of rVSV-dG-EGFP and rVSV-dG-Ferritin-EGFP. N, P, M, G and L are five VSV*
 581 *structural genes from wild type viruses; G was deleted to construct a replication-restricted*
 582 *recombinant virus, VSV-dG (van den Pol et al., 2009); EGFP or Ferritin-EGFP gene was inserted*
 583 *into VSV-dG virus genome. B and C: Results of T2-weighted (B) and T2*-weighted (C) images seven*
 584 *days after injection (left arrows, rVSV-dG-EGFP; right arrow, rVSV-dG-Ferritin-EGFP); (D)*
 585 *Fluorescent image of the same slice from the same mouse. Comparison of the T2 (E) and T2* (F)*
 586 *Normalized T2 and T2* weighted MRI signals between brain regions infected with*
 587 *rVSV-dG-Ferritin-EGFP and rVSV-dG-EGFP, Paired t-test, Ave. \pm STD; *: $p < 0.05$; **: $p < 0.01$.*

588 Fig. 2. rVSV-Ferritin-EGFP anterogradely transmitted across multiple synapses. *Note: A: Virus genomes of*
 589 *rVSV-EGFP and rVSV-Ferritin-EGFP. N, P, M, G and L are five VSV structural genes from wild type*
 590 *viruses. EGFP or Ferritin-EGFP gene was inserted into VSV virus genome; B: rVSV-Ferritin-EGFP*
 591 *was microinjected into CPU; Expected targets for anterograde spread include SN (substantia nigra,*
 592 *primary anterograde trans-synaptic target) and TH (thalamus, secondary anterograde trans-synaptic*
 593 *target); C-E: The neurons in CPU, SN and TH were labeled with EGFP, suggesting that*
 594 *rVSV-Ferritin-EGFP spreads anterogradely along the synaptically connected network as expected.*

595 Fig. 3. The signals in MRI and fluorescent images in both rVSV-EGFP and rVSV-Ferritin-EGFP animals
 596 four days after the virus injection into the SC. *Note: The brain (with skull) was removed and imaged*
 597 *with MRI scanner, and then the coronal slices were utilized for fluorescent imaging. Upper in both*
 598 *groups, fluorescent images; lower, MRI images; red box, the injection site.*

599 Fig. 4. Comparisons of the normalized MRI signals in the virus infected areas in the FerritinEGFP and
 600 EGFP groups. *Note: A: Locations of the segmented selected regions (Auditory cortex (AuC)_right (R),*
 601 *Caudate Putamen (CPU)_Left (L), CPU_R, Hippocampus (Hipp)_L, Hipp_R, Motor Cortex (MC)_L,*
 602 *MC_R, RSC_R, Somatosensory Cortex (SC)_L, SC_R, Thalamus (TH)_R, Visual Cortex (ViC)_R) on*
 603 *the structural MRI images; B: Comparisons of the normalized MRI signals in the virus infected areas,*
 604 *Olfactory tubercle_R (OT_R) and OT_L which were selected as control. Note: * $p < 0.05$, ** $p < 0.01$,*
 605 *two-tailed t-test, Ave. \pm STD, $n = 5$.*

606 Fig. 5. Co-localization of ferritin and EGFP proteins in brain regions infected with rVSV-Ferritin-EGFP.
 607 *Note: Immunohistochemistry staining demonstrates that ferritin (Red) and EGFP (Green) proteins*
 608 *express similar patterns in FerritinEGFP group. The cell nuclei (Blue) were counterstained with*
 609 *DAPI*

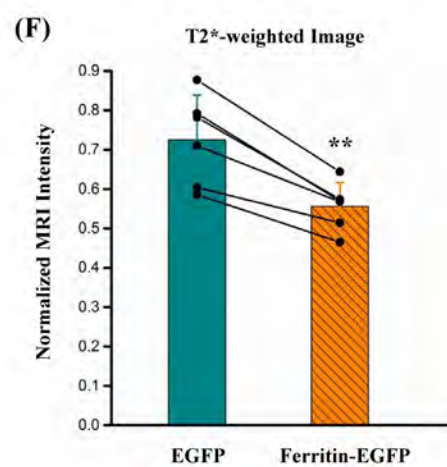
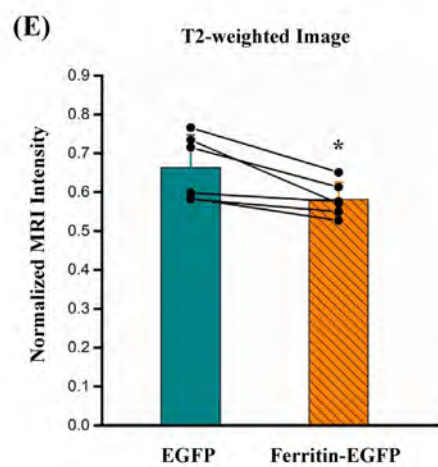
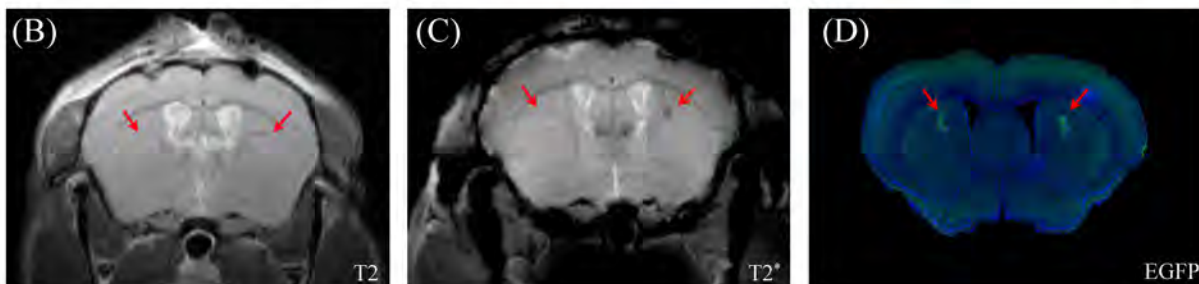
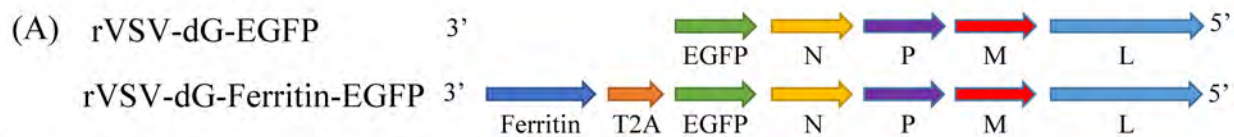
610 Fig. 6. Confocal image of AuC in FerritinEGFP group shows that ferritin (Red) colocalized with EGFP
 611 (Green) protein. *Note: The cell nuclei (Blue) were counterstained with DAPI. Scale bar = 100 μ m.*

612 Fig. 7. Increased iron accumulation in brain regions infected with rVSV-Ferritin-EGFP. *Note: A-B: In*
 613 *FerritinEGFP group, Perls' Prussian Blue staining reveals obvious iron accumulation in the injection*
 614 *site. C-H: Presence of Fe^{3+} in several brain regions (SC, CPU, Hipp, ViC and TH) that displayed*
 615 *hypointense contrast in MRI images. I: OT was selected as the control region for comparison, where*
 616 *MRI signal was not significantly changed. There was lack of obvious positive Perls' Prussian Blue*
 617 *staining positive area in OT. Scale bar = 300 μ m.*

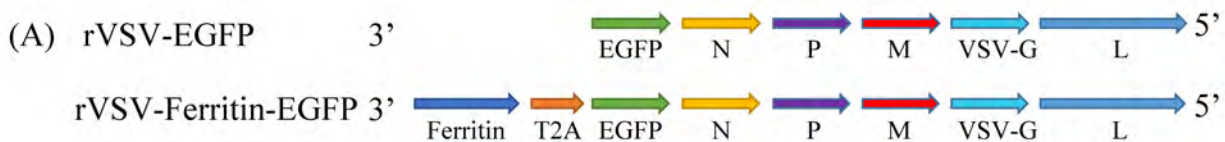
618 Fig. 8. The relationship between the green fluorescent signal intensity in the FerritinEGFP group and the
 619 ratio of the difference in normalized MRI signal intensities between groups (EGFP and FerritinEGFP)
 620 and the normalized MRI signal intensities in the EGFP group ($(S_{EGFP} - S_{FerritinEGFP}) / S_{EGFP}$). *Note: A*

621 *linear trend line was drawn for RSC_R, CPU_R, MC_R, AuC_R, TH_R and ViC_R, $y = 0.4494x +$*
622 *0.1302 ($R^2 = 0.5904$)*

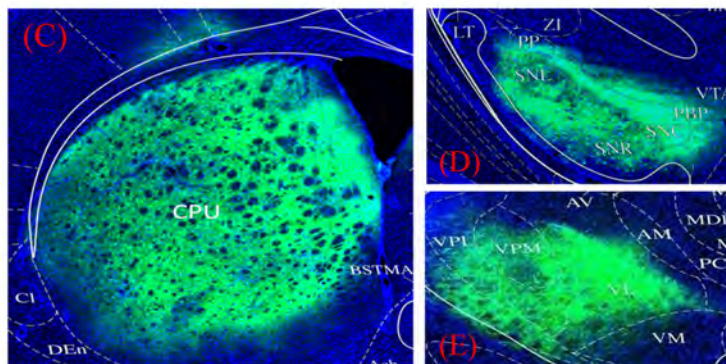
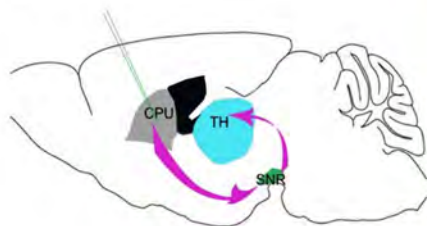
ACCEPTED MANUSCRIPT



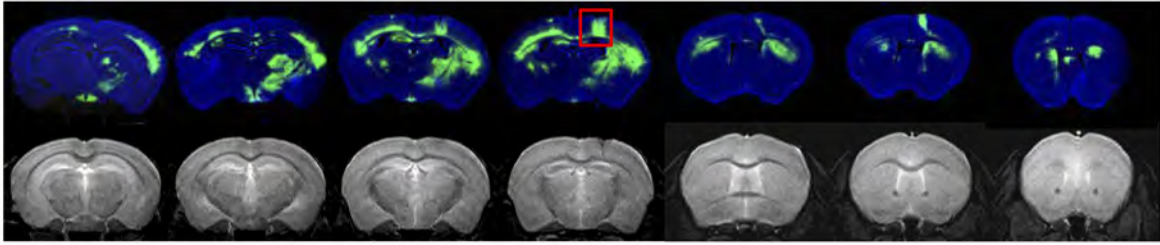
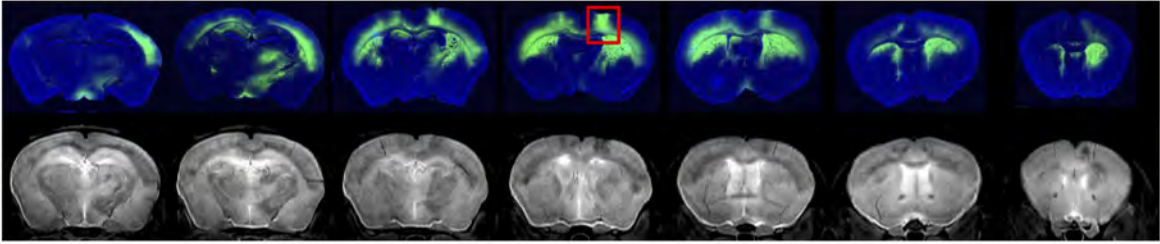
ACCEPTED



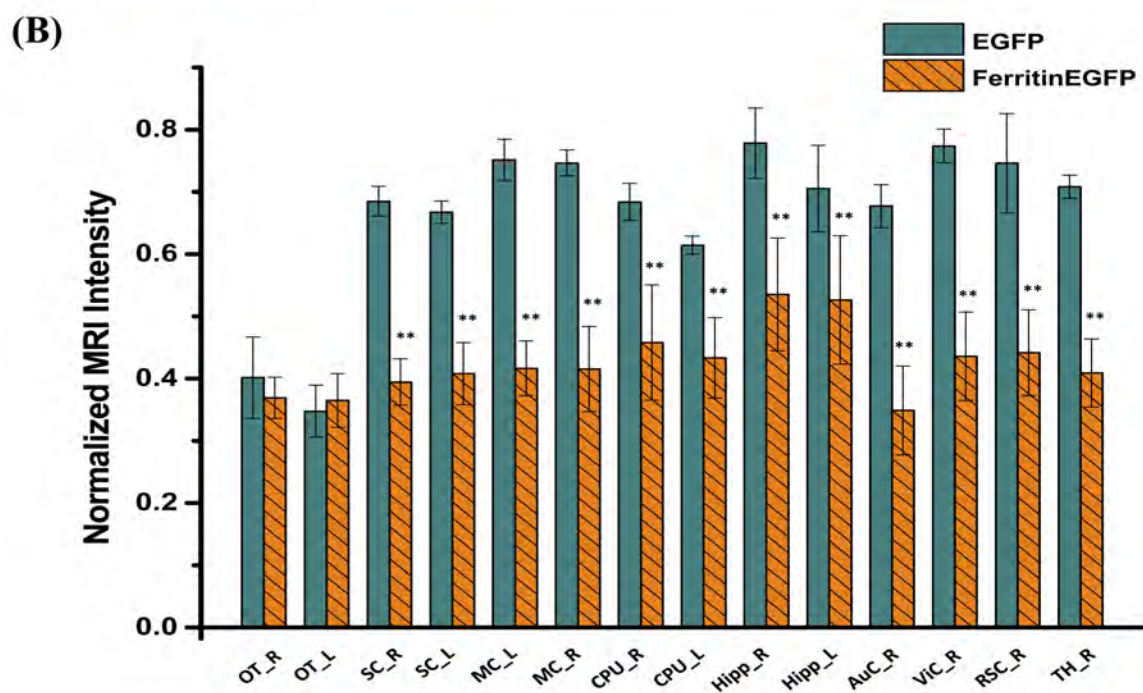
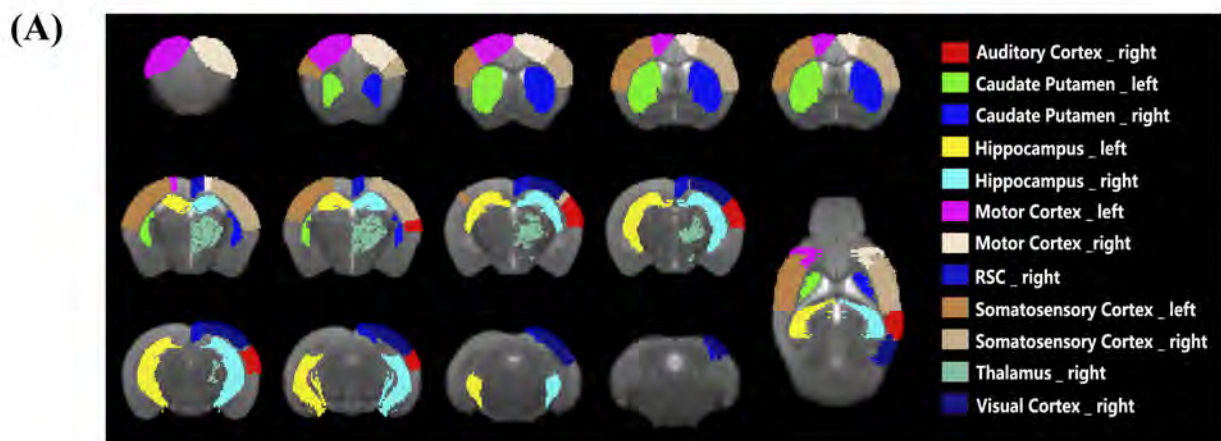
(B)



ACCEPTED MANUSCRIPT

EGFP**FerritinEGFP**

ACCEPTED MANUSCRIPT



Red: Ferritin**Green: EGFP****Merge****Blue: DAPI**